Proceedings of ASME Turbo Expo 2011
GT2011
June 6-10, 2011, Vancouver, British Columbia, Canada

GT2011-46363

AERODYNAMIC IMPROVEMENT OF A TRANSONIC FAN OUTLET GUIDE VANE USING 3D DESIGN OPTIMIZATION

Giles Endicott
Honda Research Institute Europe GmbH
Carl-Legien-Str.30
D-63073 Offenbach/Main, Germany

Toyotaka Sonoda
Honda R&D Co.
Aircraft Engine R&D Center
1-4-1 Chuo, Wako-shi, Saitama 351-0193, Japan

Markus Olhofer
Honda Research Institute Europe GmbH
Carl-Legien-Str.30
D-63073 Offenbach/Main, Germany

Toshiyuki Arima
Honda R&D Co.
Fundamental Technology Research Center
1-4-1 Chuo, Wako-shi, Saitama 351-0193, Japan

ABSTRACT

In this paper we follow the process of rapid design improvement for the fan outlet guide vane for a turbofan powering a very light jet. The small size of such engines leads to a low Reynolds number, resulting in flow-fields prone to boundary layer separation, causing significant losses in efficiency. This paper studies experimental testing in a scale rig, and numerical simulation using CFD, leading to the comparison of the two datasets and hence assessment of the numerical technique. The mesh employed by the CFD simulation was modified using Free Form Deformation to create different geometric designs, and hence an optimization scheme was subsequently utilized to find the deformation of 28 variables which maximized aerodynamic performance. The final optimized design displayed a novel oscillatory casing profile, while the blade shape had increased camber relative to the baseline. The improvement in pressure loss was approximately 20% across the range of operating conditions studied.

NOMENCLATURE

C	airfoil chord
Cp	specific heat at constant pressure
M	Mach number
p	static pressure
Po	total pressure
R	gas constant
r	distance in radial direction
To	total temperature
U	blade speed
v	flow velocity
X	distance in axial direction
γ	ratio of specific heat capacities Cp/Cv
ρ	density

Subscripts

1	inlet station of upstream of rotor leading edge
2	outlet station of rotor / inlet station of OGV
3	outlet station of downstream of OGV
ax	axial
is	isentropic process value
tip	blade tip
θ	angle in circumferential direction

Abbreviations

CFD	computational fluid dynamics
EXP	experiment
FFD	free form deformation
LE	leading edge
OGV	outlet guide vane
TE	trailing edge

INTRODUCTION

Aviation gas turbines have reaped the benefits of adding a bypass system to their design through extracting energy from their exhaust stream to power a high mass flow fan. In doing so, these engines increase their propulsive efficiency, that is, they convert a higher proportion of the mechanical energy

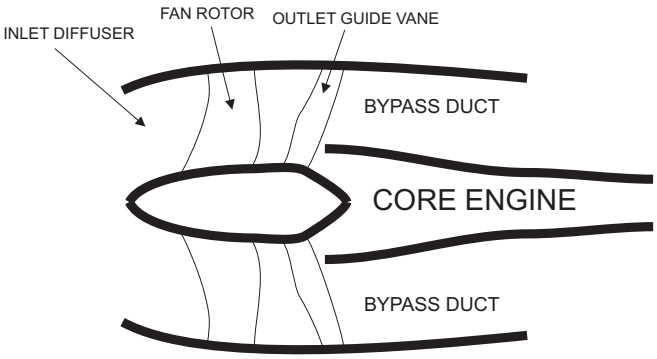

Fig. 1 Schematic of turbofan bypass section layout

Fig. 2 Turbofan engine installed into a very light jet

contained within the engine to thrust and additionally they significantly reduce the amount noise produced from the expelled exhaust jet. Due to the relationship between exhaust velocity and propulsive efficiency, the ratio of air passing through the bypass fan system undergoing only a modest velocity increase compared to the core engine has increased in the past decades to increase efficiency further.

At the historic onset of the turbofan, the bypass system's mass flow was roughly equal to the mass flow of the core engine, while for today's state of the art turbofans this ratio is close to ten in favor of the bypass fan flow. The design of a typical modern turbofan is shown in Fig. 1, ignoring the details of the core engine. The fan rotor, powered by a low pressure turbine within the core engine increases the stagnation pressure of the incoming air from the upstream diffuser. As a result the flow direction is significantly transferred from the axial to circumferential direction and if it remained in this direction it would not contribute toward the engine's thrust, which relies exclusively on the velocity component in the axial direction. To counter this, behind the fan rotor lies a row of stator blades (Outlet Guide Vane: OGV), with the purpose of converting the circumferential motion toward the axial direction with the aim of creating uniform axial flow downstream, to maximize thrust and hence minimize aerodynamic losses. Significant considerations of the design of these OGVs have been performed in past decades, studying blade shape [1], stagger [2], lean [3], sweep [4] together with the shape of the passage that contains them, in both symmetrical and asymmetrical forms [5].

In this paper we follow one stage of the continual design improvement process of a small turbofan for the very light jet market. With takeoff thrust in the region of 10kN, in comparison with more common airliner turbofans of 100-400kN, the dimensions are significantly smaller, with the engine diameter approximately half a meter, one sixth of the diameter of the largest turbofan engine today. As a result, the Reynolds number of the internal flow is smaller to the same ratio, resulting in a less stable boundary layer more prone to flow separation with the potential to cause problems in creating blade designs which are able to cope with a wide range of operating conditions. The compressor stage under investigation in this study is located within the fan stage of a modern small turbofan engine for a very light business jet, shown in Fig. 2.

We concentrate on the design improvement of the OGVs in which initially we perform experimental testing on a small scale rig to ascertain the current design performance. Using computational fluid dynamics, we present a simulation strategy capable of simulating the flow-field around the OGVs. We move on to critically compare and contrast the experimental and computational results, with the aim of being able to confidently use the computational simulations to accurately create a testing environment for new OGV design concepts.

Given a simulation technique that can accurately recreate the physics of the real world, the application of computational design can lead to significant improvements to in service performance without the need for intensive human intervention. Computational design or design optimization, pioneered in the aerospace domain in 1978 [6] with the numerical design of transonic wings has progressed to a popular technique for the development of turbomachinery in the current era. While early simulation methodologies pushed computational resources to their limits, allowing only several simulations to be performed in a given time frame, today steady state simulations are easily within the reach of commodity hardware, allowing optimization technologies to be applied to the results of simulations. We demonstrate such a technology within this paper in order to find new design concept which deliver increased aerodynamic performance.

Design optimization involves a shift of the design process from the engineering domain to a mathematical domain through several processes. We convert the performance of a design from engineering perspectives to a single or multiple objective values, generally of a continuous nature. These are obtained from one or many simulations performed which analyze the design performance in one or many engineering domains, e.g. aerodynamics, structure, noise etc. To facilitate the design variation, in order to test many possible designs, the geometry (or alternatively operating conditions, settings etc.) must be transferred to a condensed numerical form. Popular techniques can be roughly split into two streams; synthesis and deformation. In the former, a geometric system builds a design

entirely with the parameters varying the construction while for the latter, a base design is specified and manipulated in some form to create a new perturbed design. In this paper we use the latter technique, given the presence of an existing acceptable design with which to perturb. The optimization process serves to find the perturbation which creates the best performance. As the process is computational, the manpower required is small, leading to an efficient process assuming the computer simulations are accurate when compared to the real world physics. It is the process of checking this correlation which leads us to the next section, experimental testing of the engine.

Design Intent

The performance map of the fan system investigated in this research is shown in Fig. 3. The top and bottom figures are of stage efficiency and stage total pressure ratio respectively, where all parameters, such as mass flow rate, efficiency, total pressure ratio, are normalized by the value at the peak efficiency point at the cruise design condition. The target of this project is to increase the peak stage efficiency at the cruise (design) point, while maintaining or improving the current surge margin. Therefore the OGV design optimization was carried out at the three design points denoted by P1 (point 1), P2 (point 2), and P5 (point 5) corresponding to "near choke", "peak efficiency", and "near surge", respectively, as shown in Fig. 4 where all data is again normalized by the loss value of the peak efficient point (point 2). It has been presumed that satisfying the cruise point discussed would bring a positive effect at the other two points (take-off, max-climb) in addition. Each value for OGV loss has been obtained from the overall (both circumferential and span-wise) mass averaged total pressure loss coefficient. The OGV loss is gradually increased as the mass flow rate is decreased, but there is a sudden increase of the OGV loss when the mass flow rate is slightly increased. Again, the target was to increase the stage efficiency by reducing the OGV loss coefficient as much as possible. Also it is required that the OGV loss reduction should be obtained for all the flow rate range from the near choke to the near surge side in order to keep or improve the current surge margin. Here, a 20% OGV loss reduction corresponds to a 0.5 % stage efficiency increase.

Objective Function and Constraints

By simulating three operating conditions, a level of robustness is invoked in the final design, as a chosen design must perform well across the operating range to achieve a good overall objective. The peak efficiency condition (point 2) is the most significant and weighted by 0.6, while the near surge condition (point 5) is assigned by a weight of 0.3 and the near choke (point 1) 0.1. The sum of these values is then taken as an overall measure of the pressure loss of the blade across its working conditions. In addition to the pressure loss values, outflow angle is additionally an important consideration. A good design is expected to have an average square value of outflow angle smaller than 2.0 (this means the averaged exit flow angle variation is about ±1.4 degree) to ensure it succeeds at its task of converting circumferential flow to axial flow.

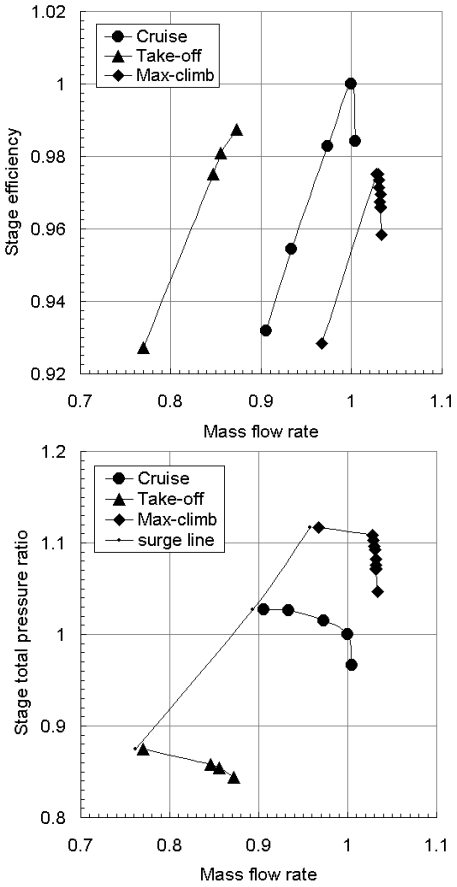

Fig. 3 Normalized fan stage performance map (top: efficiency, bottom: total pressure ratio)

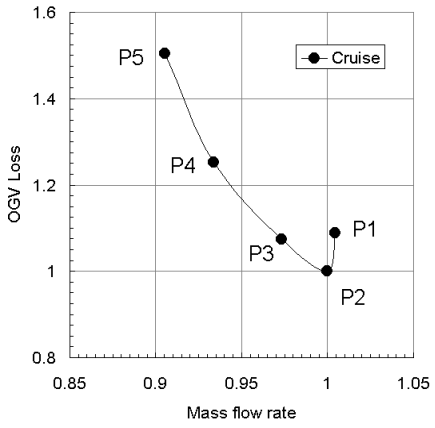

Fig. 4 Normalized OGV total pressure loss coefficient at point 2, cruise condition

EXPERIMENTAL METHODS

The first stage of the design process was to accurately gauge the existing performance to form a benchmark from

which to improve. In our case, such a process is best performed experimentally to ensure accuracy. The experiments were performed in a small scale high-speed single stage research compressor at the Honda Aircraft Engine R&D Center (see **Fig. 5**). At the peak efficiency point in the cruise condition the OGV inlet Mach number and the turning angle at the hub are approximately 0.9 and about 50 degrees, while at the tip they are approximately 0.7 and about 55 degrees. In order to reduce the shock loss at the hub the OGV leading edge was swept forward toward the hub. At the tip the OGV leading edge was swept forward again in order to increase solidity. The solidities at the hub and the tip are 2.8 and 1.8, respectively.

In the experimental rig, ambient air is led through a bell-mouth and a settling chamber with flow conditioning screens and a contraction before entering the compressor stage. The rotor is driven by a 300KW DC-drive with the shaft speed and power measured using a torque-meter. The mass flow rate is measured at the bell-mouth while the inlet total pressure and temperature are measured by probes located inside the settling chamber. The stage exit total pressure and temperature are measured by tandem probes located downstream of the OGV. Two tandem probes for total pressure measurement and two tandem probes for total temperature measurement are circumferentially distributed and traversed in the circumferential direction by a traversing ring concurrently in order to estimate the circumferential variation of the experiments. The OGV exit flow angle is obtained from a single five-hole probe installed to the traverse ring where the probe is circumferentially traversed at each span-wise position. Simultaneous measurement using the tandem probes and the five-hole probe was not possible, therefore they were carried out separately. As the compressor characteristics are significantly changed when the probes are inserted to the passage downstream of the rotor and upstream of the OGV, only static pressure at the casing wall was measured between the rotor-TE and OGV-LE.

As a result of having no flow-field measurements between the rotor and OGV, the inlet boundary conditions for the OGV blade need to be predicted using the measured data together with some assumptions. The inlet total pressure of the OGV was assumed to be equal to be the maximum value of OGV wake. On the other hand, the inlet total temperature of OGV was assumed to be equal to be the mass averaged value of OGV wake. These assumptions have been also used by Wennerstrom's high-through flow transonic axial compressor stage **[7]** where the similarly swept OGV has been installed and tested. Also, the OGV-CFD results show that this assumption on the "inlet total pressure" is reasonable (not shown here). It therefore seems that the sweep incorporated in the OGV leading edge around the hub appears to entirely eliminate shock losses. The inlet flow angle of the OGV was calculated by applying the Euler turbine equation to the rotor and the simple radial equilibrium equation to the OGV inlet using an iterative procedure. This is as follows:

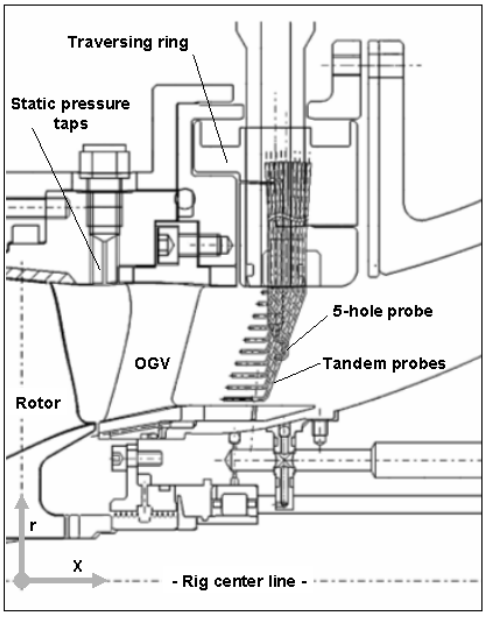

Fig. 5 Small scale high-speed single stage research fan compressor rig

(1) Set $To_2(r) = To_3(r)$, $Po_2(r) = Po_3(r)$.

(2) Calculate $v_{2\theta}(r)$ profile using
$Cp\left(To_2(r) - To_1(r)\right) = U\left(v_{2\theta}(r) - v_{1\theta}(r)\right)$.

(3) Assume pressure profile $p_2(r)$.

(4) Compute Mach number profile $M_2(r)$ using
$$M_2(r) = \sqrt{\frac{2}{\gamma - 1}\left\{1 - \left(\frac{p_2(r)}{Po_2(r)}\right)^{\frac{\gamma-1}{\gamma}}\right\}}.$$

(5) Compute density profile $\rho_2(r)$ using
$$\rho_2(r) = \left(\frac{Po_2(r)}{R \cdot To_2(r)}\right) \Bigg/ \left(1 + \frac{\gamma - 1}{2} M_2(r)^2\right)^{\frac{1}{\gamma-1}}.$$

(6) Update pressure profile $p_2(r)$ using
$$p_2(r) = p(r_{tip}) - \int_r^{r_{tip}} \rho_2(r) \frac{v_{2\theta}(r)^2}{r} dr.$$

(7) If pressure profile is not converged then repeat from step (4)-(6).

The measurement accuracy is, as follows. The loss coefficient uncertainty for a single wake is determined to be ± 0.1 percent However, due to circumferential variability of the wake, the maximum uncertainty for the overall mass averaged loss coefficient from P1 (near choke) to P5 (near surge) is estimated as ± 0.6 percent. The exit flow angle is ± 0.5 degree.

COMPUTATIONAL METHODS

For the simulation of the fluid dynamic properties of the blade designs we used the parallelized 3D in-house Reynolds-

averaged Navier-Stokes (RANS) flow solver HSTAR (Honda Software for Turbomachinery Aerodynamics Research) [8]. For turbulence modeling, Menter's k-ω SST turbulence model [9] was chosen through CFD assessment for the baseline blade geometry in comparison with the experimental results. In order to sufficiently resolve the boundary layer development, CFD simulations were performed prior to the optimization to determine the number of cells required to obtain grid independence. The chosen computational grid consisted of 201 nodes in the stream-wise direction, 81 nodes in the radial direction, and 61 nodes in the circumferential direction (totaling approximately one million cells). The average y^+ of the first grid point from the wall is close to 1.0 for all calculations. The computational grid for the baseline blade is shown in Fig. 6. The computation time for one flow analysis with this grid takes roughly 50 minutes on an Intel Xeon5570 2.93 GHz Quad-Core processor using the Intel MPI library.

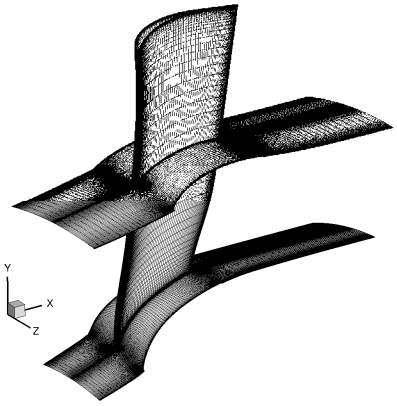

Fig. 6 Structured computational mesh

ASSESSMENT OF CFD CODE

An assessment of the results comparing experimental and simulated total pressure loss for the for the baseline OGV are shown in Fig. 7. The top figure (Fig. 7 (a)) shows a comparison of the span-wise stage total pressure ratio where the concrete-absolute value of the horizontal axis is not shown here, but only "gauge" values are shown. The legend entries of "EXP wake-1" and "EXP wake-2" correspond to measured values at two different circumferential positions, obtained from the two tandem total pressure probes, as mentioned previously. It can be seen that there is a good agreement between experimental (EXP) and computational results (CFD), although experimental variability is observed around 10% and 80% span-height, where the effects of OGV hub secondary flow and rotor tip leakage vortex respectively are particularly large. The middle figure (Fig. 7 (b)) shows the comparison of normalized overall OGV total pressure loss as a function of the normalized mass flow rate at the cruise operation condition. The two performance estimation techniques (EXP and CFD) agree both qualitatively and quantitatively, again. The bottom figure (Fig. 7 (c)) shows the comparison of OGV span-wise exit flow angle. A good qualitative agreement is obtained, although there is a discrepancy of between 1 to 2 degrees. In summary, there is a good correlation between EXP and CFD.

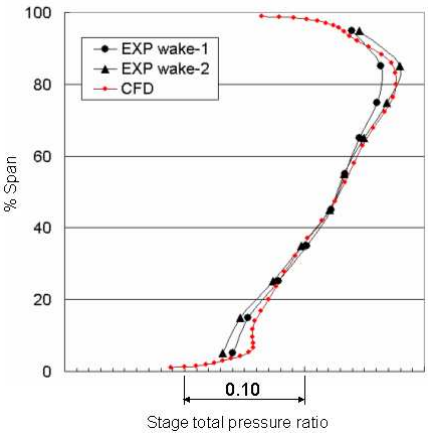

(a) Span-wise stage total pressure ratio at P2

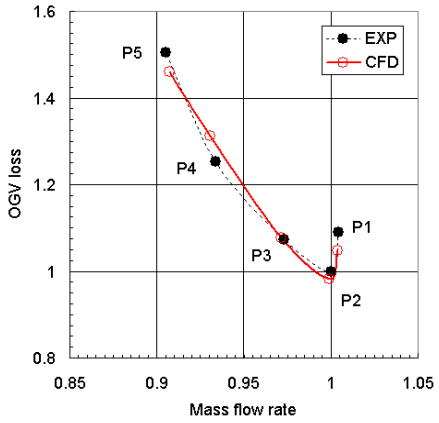

(b) Normalized OGV loss

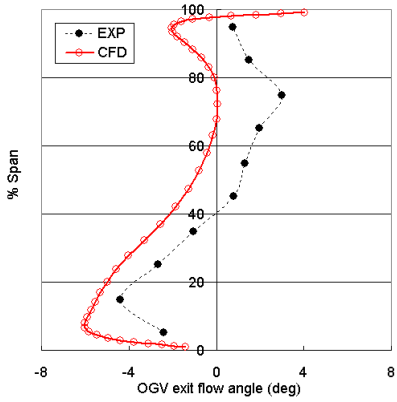

(c) Span-wise OGV exit flow angle at P2

Fig. 7 Experimental and numerical comparison for Baseline OGV at cruise condition

OPTIMIZATION METHODOLOGY

The optimization of the OGV will be performed using the CFD simulation discussed in the previous section in order to find a geometric design superior to the baseline.

The manipulation of the blade and passage geometry enabling the shape optimization will be performed using free form deformation (FFD). Pioneered by Sederberg and Parry [10] in 1986, the method provides a user intuitive form of shape modification, analogous to the compression and expansion of the design formed in rubber as shown in Fig. 8. Using this method the geometry, defined as a set of co-ordinates in space is embedded within a parametric volume defined by the Euclidean position of a set of control points. In the original manifestation of FFD, strict rules applied for the layout of these control points so that they create a regular parallelepiped grid. Extensions to the method [11,12] have resulted in the possibility for a more arbitrary layout of the control points to which the geometry is embedded. While FFD was originally conceived as a graphics and animation tool, its potential for application in engineering and in particular design optimization was soon realized using local [12] and evolutionary global search [13] methods.

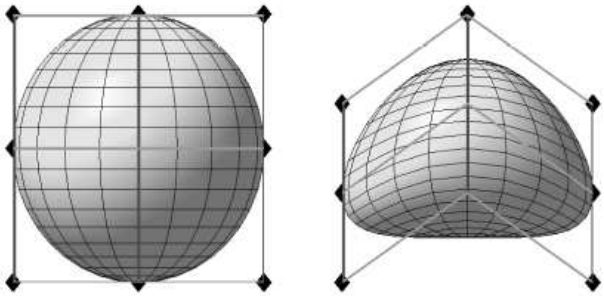

Fig. 8 Free form deformation of a sphere

One advantage of FFD is the speed at which it can be applied to a pre-existing aerodynamic simulation. Instead of the need for producing a reliable and repeatable software method for creating new meshes for each design variation, the deformation process can be applied directly to the nodes which form the CFD solution mesh. Additionally as the mesh topology remains constant, the level of discretization noise in the objective landscapes is significantly reduced. In this paper we apply FFD on the OGV passage mesh, comprising of approximately one million node points.

The FFD grid for the OGV passage as shown in Fig. 9 comprised of 6 control points in the axial direction, 4 points in the circumferential direction and 4 points in the radial direction which formed a control volume encompassing all node points tightly. Control points were then grouped together and moved in a coordinated fashion to form design variables linked to the shape of the passage and blade. For the hub and casing wall contours, eight groups (four hub and four casing) were formed with each comprising of all four control points in the circumferential direction for each of the axially internal control points on the radial limits of the control volume. These groups were linked to design variables which allowed their movement in the radial direction. Blade variables were formed grouping control points on each of the four span-wise planes, leading to control of leading edge and mid-chord thickness, and leading edge, mid chord and trailing edge circumferential position. In all 28 variables were created for the optimization process. Limits were placed on the deformation to ensure a low number of failures of the mesh as a result of its manipulation. However, this led to only small deformations of the blade shape being possible, however the passage shape was still highly variable without fear of mesh failure, and was hence limited mainly by design constraints.

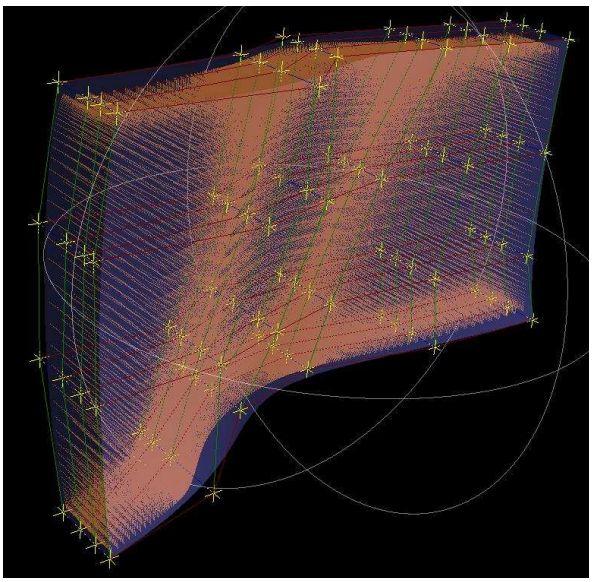

Fig. 9 OGV passage mesh node points (orange) an FFD control grid

With the geometric variation scheme developed, the task now falls to choosing the set of input parameters for the geometry that maximizes our objective function which reflects aerodynamic performance. The use of global search methods is popular for its ability to search throughout an entire hyperspace for optimal solutions without significant consideration of the starting point. In this paper we apply the method of differential evolution [14]. Differential evolution is a newcomer in the wide catalogue of global search techniques including genetic algorithms, evolution strategies, particle swarms etc. Mutation based upon the variations between different designs in the current population employed together with crossover form the main innovation in this algorithm with respect to its counterparts in the field.

As the turnaround time of design optimization is key to its applicability in industrial design, it is important to control the time required for the optimization process. The number of design evaluations required for convergence of the global

search process using CFD evaluations directly can be very high, of the order of many thousands and with some simulations taking many tens of processor hours each, the time required to employ optimization methodology can easily become too long to fit within the overall industrial design process. Surrogate assisted optimization can provide assistance with this problem. By building a model of the objective landscape, an optimization algorithm can be applied to this model in lieu of running a full CFD calculation assuming a sufficiently accurate model can be built using data from a smaller number of simulations than a direct global search requires. In order to build the best possible model with the least number of CFD calculations, an iterative approach is taken to progressively increase the accuracy of the model in regions of interest within the design space.

Initially a model is built using a sampling plan of simulations sized approximately ten times the number of design variables [15] using an optimized Latin-Hypercube sampling plan [16]. In this case an initial model was built from the successful 386 simulations of a 400 point sampling plan. Kriging based surrogate models [17] were built for each design objective and constraint by tuning internal parameters to form a maximum likelihood estimation using the combination of differential evolution and hill climbing. With each model built, a constrained objective could be built for any parameter set through the use of ramped penalty functions for constraining the exit flow angle and maintaining geometric limits and adding this to the weighted pressure loss objective so that the minimum value of this combined objective obeys all constraints.

Instead of predicting the true value of the pressure loss objective, the expected improvement is used [18]. This is the expected value of the improvement upon the current best value, taking in to consideration the local error estimate. It serves to push the search process to areas where the standard prediction suggests non-optimal performance but a high prediction error means good performance is possible within the error bounds. As a result a better balance of exploration and exploitation is found in the search, which tends to exploitation as error bounds become smaller.

Differential evolution is used with the model of the combined objective function to find the set of parameters that result in its minimum. This result is subsequently further converged by a simple hill climbing technique. Given the best result from the hill climb and a further twenty four of the best parameter sets from the final population of the differential evolution, CFD calculations using these design parameters can be performed to add the results of predicted optima to the database for model construction. The model can then be rebuilt and searched again and then repeated until the allowable budget of simulation or time is reached. In this case, the process was repeated ten times, giving a total of 250 simulations in addition to the original sampling of 400 simulations.

RESULTS AND DISCUSSION

In this section we discuss the results of the optimization process described previously, and report the aerodynamic characteristics of the best design found by the optimization process. In Fig. 10 (a) the weighted pressure loss is shown for each of the simulations performed for the optimized blade, in comparison with the baseline. The optimal design found shows an improvement of about 20% in terms of total pressure loss reduction (0.5% efficiency increase) at the peak efficiency condition (point 2) and also at the other operating points. The steep increase of loss at the choke point is also improved. Due to the uniform loss reduction across the whole range of operating conditions it appears that the surge margin is at least not worse than the baseline. On the other hand, Fig. 10 (b) shows the span-wise OGV exit flow angle distribution for the baseline and the optimized OGVs. The minus sign denotes "under-turning" of the OGV exit flow angle. In the case of the optimized OGV, the aerodynamic loading is increased, but the losses for the optimized OGV are lower than the baseline. The reason why the optimized OGV is superior to the baseline OGV is discussed in the following section.

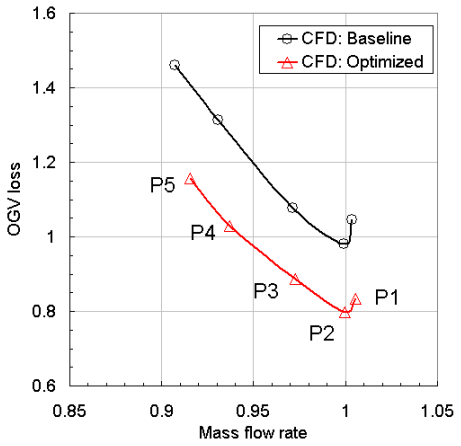

(a) OGV total pressure loss

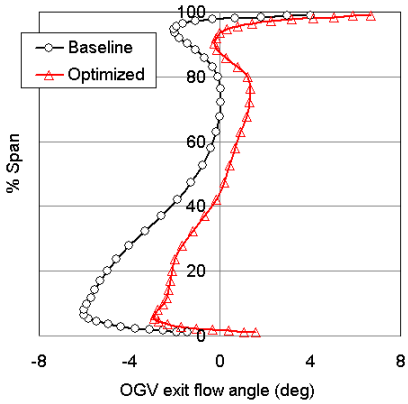

(b) OGV exit flow angle

Fig. 10 Numerical results of (a): total pressure loss and (b): exit flow angle for Baseline and Optimized OGV

The optimal passage and blade geometries are shown in Fig. 11 (a) and (b), respectively. In comparison to the baseline, the passage has been significantly moved radially outward, together with modifications to the passage profile. The optimal design incorporates an unconventional oscillatory profile with the maximum passage area at around 20% of the OGV chord, before a significant contraction, with minimal area close to the trailing edge. The variation in the blade profile geometry is visualized with three profiles at span heights of 5, 50, and 95% of the span from hub to casing in Fig. 11 (b). The deformations are small and have mainly added additional camber to the airfoil, and additionally toward the tip the stagger angle is reduced slightly as the camber is added.

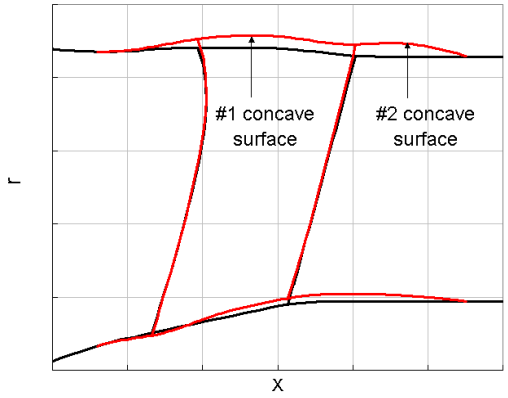

(a) Meridional passage

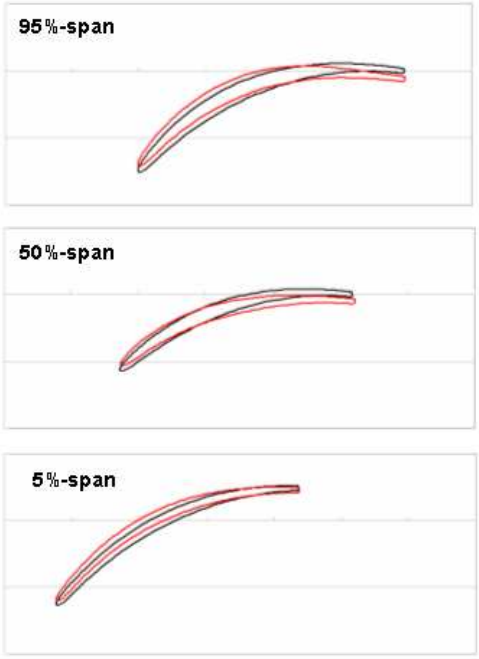

(b) Blade airfoil

Fig. 11 Comparison of meridional passage geometry (top) and blade airfoil geometry (bottom), Baseline: black, Optimized: red

The isentropic Mach number distribution on the airfoil surface at the peak efficiency condition for 5, 50, and 95% span-heights for both the baseline and optimized blades is shown in Fig. 12. For all spans, the optimized blade has shifted the maximum Mach number, and hence minimum pressure position forward on the chord. This is especially true for the blade extremities (5% and 95% span height) while the changes at mid-span are more subtle. It seems that a more front loaded airfoil is effective in reducing the profile loss.

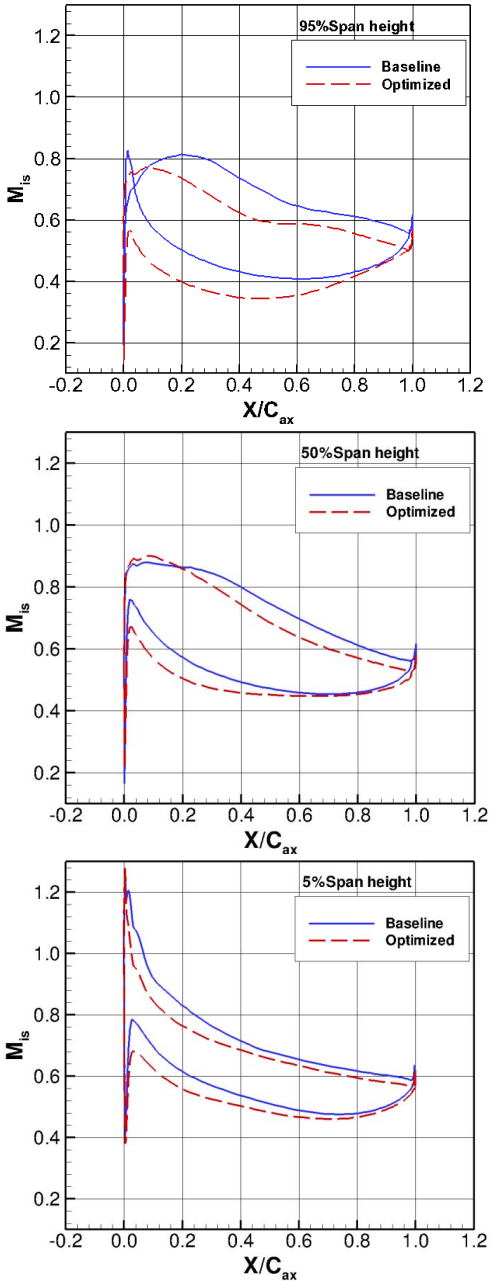

Fig. 12 Isentropic Mach number distribution for Baseline (blue) and Optimized (red) at three span heights, top: 95% span, middle: 50% span, bottom: 5% span

Surface limited streamlines of the suction side of the OGV as shown in Fig. 13 which enable us to visualize the flow along the blade and analyze the existence of secondary flows at the extremities of the blade. On the baseline blade a very large region of separated, secondary flow is visible on the trailing edge near the hub up to 58% of the span. In the optimized blade this has been reduced to 39% of the span. However separation in the proximity of the casing has increased from 12% of the span to 21%. Overall the optimized blade includes a larger region of tidy flow in the mid-span, explaining some of the improvement in pressure loss. It seems that a span-wise pressure gradient from casing to hub generated by the second concave surface in the oscillatory casing profile plays an important rule.

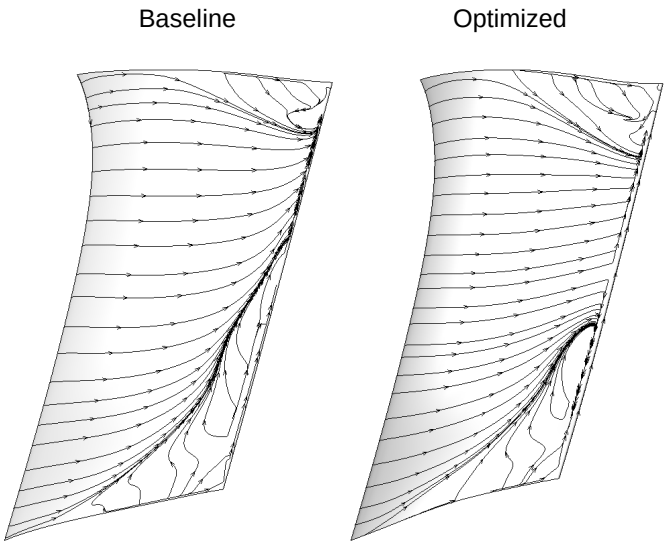

Fig. 13. Comparison of numerical oil flow pattern on OGV suction surface, left: Baseline, right: Optimized

CONCLUDING REMARKS

In this paper we have demonstrated the computational design improvement of the OGV section of a small turbofan by first evaluating the real world performance of the blade system, and subsequently successfully building a computational model that can reproduce the results. Using this computational aerodynamics model, optimization was performed to find a more optimal design, while staying robust to the changes in flight conditions. The final design showed an improvement of pressure loss approximately 20% in the weighted system.

However the CFD assessment process prior to the optimization only demonstrates the validity of the model to the baseline design. It follows that the next stage of this project is to manufacture this blade for the purpose of undergoing the same experimental procedure as was applied for the baseline blade. Only this can determine the true merit of the suggested design. At the time of writing of this paper, this was yet to be achieved; a reality of the high costs and time commitment of experimental testing which has driven the growth of computationally design methods.

ACKNOWLEDGEMENTS

The authors would like to express their gratitude to Hideo Otani and Hisato Tanaka from the Honda R&D who performed the test program and transmitted the baseline OGV geometry data, respectively.

REFERENCES

[1] Lee, S.Y. and Kim, K.Y., "Design Optimization of Axial Flow Compressor Blades with Three-Dimensional Navier-Stokes Solver". Journal of Mechanical Science and Technology **14 (9**), pp. 1005-1012.

[2] Yoon, Y.S., Song, S.J., and Shin, H.W., 2006. "Influence of Flow Coefficient, Stagger Angle, and Tip Clearance on Tip Vortex in Axial Compressors" Journal of Fluids Engineering. **128**, pp. 1274-1283.

[3] Harrison, S., 1992, "The Influence of Blade Lean on Turbine Losses", Journal of Turbomachinery." **114**, pp. 184-191.

[4] Jang, C.M., Li P. and Kim, K.Y., 2005 "Optimization of Blade Sweep in a Transonic Axial Compressor Rotor", JSME International Journal Series B, **48 (**4), pp. 793-801.

[5] Gregory-Smith, D.J., Ingram, G., Jayaraman, P., Harvey, N.W., Rose, M.G., 2001, "Non-Axisymmetric Turbine End Wall Profiling," Proceedings of the Institution of Mechanical Engineers, Part A: Journal of Power and Energy, **215** (6) pp. 721-734.

[6] Hicks, R.M. and Henne, P.A., 1978, "Wing Design by Numerical Optimization", AIAA Journal, **15**(7) pp.407-412.

[7] Wennerstrom, A.J., 1984, "Experimental Study of a High-Throughflow Transonic Axial Compressor Stage," ASME Journal of Engineering for gas turbines and Power, **106**, pp. 552-560.

[8] Arima, T., Sonoda, T., Shirotori, M., Tamura, A., and Kikuchi, K., 1999, "A Numerical Investigation of Transonic Axial Compressor Rotor Flow Using a Low-Reynolds-Number k-ε Turbulence Model," ASME Journal of Turbomachinery, **121**, pp. 44-58.

[9] Menter, F. R., 1994, "Two-Equation Eddy-Viscosity Turbulence Models for Engineering Applications," AIAA Journal, Vol., **32**(8), pp. 1598-1605.

[10] Sederberg T.W. and Parry, S.R., 1986, "Free-Form Deformation of Solid Geometric Models", SIGGRAPH Comput. Graph., **20**(4),pp151-160.

[11] Coquillart S., 1990, "Extended Free-Form Deformation: a Sculpturing Tool for 3D Geometric Modeling". SIGGRAPH '90: Proceedings of the 17th annual conference on Computer graphics and interactive techniques, pp. 187-196, New York, USA.

[12] Perry, E.C., 1999, “Three-Dimensional Shape Optimization of Internal Fluid Flow Systems using Arbitrary Shape Deformation Coupled with Computational Fluid Dynamics”. PhD thesis, Brigham Young University, Provo, Utah.

[13] Eisuke K., Hisashi T., 1997, “Shape Optimization of Continuum Structures by Genetic Algorithm and Boundary Element Method”, Engineering Analysis with Boundary Elements, **19** (2), Optimization and Sensitivity Analysis, pp. 129-136.

[14] Storn, R., Price, K. 1997, "Differential Evolution - a Simple and Efficient Heuristic for Global Optimization over Continuous Spaces". Journal of Global Optimization, **11**, pp. 341–359.

[15] Jones, D.R., 2001, “A Taxonomy of Global Optimization Methods based on Response Surfaces,” Journal of Global Optimization, **21**, pp. 345-383.

[16] Morris, M. and Mitchell, T., 1995, “Exploratory Designs for Computational Experiments”, Journal of Statistical Planning and Inference, **4**, pp. 381-402.

[17] Sacks, J., Welch, W.J., Mitchell, T.J. and Wynn., H.P., 1989, “Design and Analysis of Computer Experiments”, Statistical Science, **4**(4) pp. 409-423.

[18] Forrester A.I., Sóbester, A., and Keane, AJ., 2008. “Engineering Design via Surrogate Modelling: a Practical Guide”, Wiley, United Kingdom.